RSC Sustainability

ROYAL SOCIETY OF CHEMISTRY

PAPER

View Article Online
View Journal | View Issue

Cite this: *RSC Sustainability*, 2024, **2**, 3826

CO_2 hydrogenation on ruthenium: comparative study of catalyst supports†

Göran Baade, [a] Jens Friedland, [a] Koustuv Ray [b] and Robert Güttel *[a]

Received 13th August 2024
Accepted 31st October 2024

DOI: 10.1039/d4su00469h

rsc.li/rscsus

To achieve a significant reduction in anthropogenic CO_2 in the near future, captured carbon has to be valorized. To this end, CO_2 may be activated using H_2 to form sustainable fuels (synthetic natural gas), platform chemicals (methanol) and higher hydrocarbons (modified Fischer–Tropsch process). In this work we synthesize Ru based catalysts from various commercially available support materials and test them under lower temperatures than usually employed at various partial pressures of CO_2 and H_2 using methanation as a model reaction. The results show Ru/TiO_2, Ru/ZrO_2 and Ru/Al_2O_3 as the most active catalysts with high activity, selectivity towards methane (>95%), and stability with little to no deactivation over 80 h. These most promising catalysts are further tested and kinetic parameters determined, which find reaction orders and activation energies in agreement with literature, but differing from catalyst to catalyst, hinting at complex reaction mechanisms including the support as well as the Ru. The TOF calculated for Ru/TiO_2 at 190 °C is 5.7 s^{-1} and highlights it as the most active catalyst in this work. The study opens new and promising avenues for the valorization of CO_2, as well as a basis to compare future optimizations and advances in the field of Ru-based CO_2 conversion.

Sustainability spotlight

In accordance with the UN sustainable development goals regarding climate action (SDG 13), it is necessary to reduce net CO_2 emissions by 2030. Since the industrial – and energy sectors cannot completely pivot away from fossil fuels as raw material until 2030, it is necessary to establish carbon-neutral fossil fuel sources. The infrastructure to use methane is already in place, which makes it a candidate for energy storage and transport. The synthesis of methane from CO_2 is already well understood for centralized plants, but energy generation, H_2 electrolysis and capture of CO_2 are expected to be decentralized. It is therefore necessary to establish what a process at much lower temperatures may look like as foundation for optimization until 2030 and beyond.

1 Introduction

Climate change is one of the major motivators of contemporary science and greenhouse gases are responsible for global warming, which has potentially devastating results. Among the greenhouse gases CO_2 is the most notable, even when accounting for different global warming potentials, due to the large amounts that are emitted.[1] Recently The Sustainable Development Goals Report of the UN has highlighted the need to drastically reduce the Greenhouse Gas emissions by 2030 and be net zero by 2050 to avoid a "Climate Calamity".[2] In accordance with these sustainability goals it is necessary to take urgent action to combat climate change and its impact.

Great efforts are being made to decarbonize fossil-based industries. Among the options to reach net-zero carbon capture from exhaust gases or ambient air and the subsequent utilization (Carbon Capture and Utilization, CCU) are being investigated. As roughly half of all CO_2 emissions are emitted decentralized as opposed to relatively pure point sources, a remote Direct Air Capture (DAC) and subsequent conversion without costly transport of gaseous CO_2 is among the options with most potential and flexibility.[3] For safe and efficient decentralized utilization of captured carbon, direct hydrogenation of CO_2 at low temperatures may keep cost low and prevent potential hazards.

Ruthenium has been found to be the most active catalyst to hydrogenate CO_2 with a high selectivity towards methane.[4] It is widely understood that the support material of a ruthenium-based catalyst has a significant influence on the activity and stability during the reaction, which is why many studies have been conducted to determine the ideal support.[5–7] However, these studies usually focus on high reaction temperatures. While studies under low-temperature conditions also exist,[8–10] they usually investigate one single support material and vary the process conditions. Additionally, other works focus on the stabilization of specific active phases,[11] complex catalyst geometries[12] or the use of novel concepts like photo-assisted

[a]*Institute of Chemical Engineering, Ulm University, Ulm, Germany. E-mail: robert.guettel@uni-ulm.de*

[b]*Department of Chemical Engineering, Indian Institute of Technology Kharagpur, Kharagpur, India*

† Electronic supplementary information (ESI) available. See DOI: https://doi.org/10.1039/d4su00469h

catalysis.[13] The reported results, while promising, are likely far from widespread application in the short timeframe left to drastically reduce net CO_2 emission. Therefore, it is necessary to close the knowledge gap in the application of different support materials in the low-temperature CO_2 hydrogenation and gain a base-line understanding of what is readily achievable on Ru with commercially available materials.

In this study we investigate the activity and selectivity of a selection of ruthenium-based catalysts in the CO_2 hydrogenation reaction. The catalysts are synthesized using commercial grade materials and a facile synthesis to minimize interference stemming from the procedure itself. All catalysts are tested under mild conditions by varying temperatures and partial pressures to form a quantitative understanding of the most promising candidates. These results are corroborated by subjecting the most promising catalyst materials to additional experiments to determine kinetic parameters for comparison with existing literature data and as a basis for further investigations.

2 Experimental

2.1 Catalyst synthesis and characterization

Six commercial grade support materials are used as received, among these are three reducible metal oxides: TiO_2 (P25 – Evonik), ZrO_2 (IBU-tec) and CeO_2 (IBU-Tec) as well as two irreducible metal oxides: Al_2O_3 (Aeroxide Alu 130 – Evonik) and SiO_2 (Aerosil 380 – Evonik) as well as one activated carbon support (IAC 402 – Infiltec). All supports are pressed into pellets, crushed and sieved to a size fraction of 150–200 μm before use to ensure comparability during the impregnation step.

The catalysts are prepared by excess solvent impregnation in which the support is poured into a solution of the Ru precursor ruthenium(III) chloride hydrate (38.0–42.0% Ru basis, Sigma-Aldrich) in water to yield a nominal mass loading of 1% Ru on the final catalyst. The solution is placed in an oil bath heated to 323 K and stirred until all solvent has evaporated. The resulting powder is placed in an oven an dried at 378 K over night, followed by calcination at 473 K for 4 h in static air. After cooling down to room temperature the samples are washed three times with dilute ammonia (3 wt%) solutions and then three times with water. This was shown to facilitate the removal of residual chlorides and thus increase activity of the catalysts.[14] After drying of the materials at 378 K, the dry powders are again pressed into pellets, crushed and sieved to a size fraction of 150–200 μm to prevent heat and mass transfer limitations during the reaction experiments.

The catalysts are subsequently characterized (3Flex, Micromeritics) by N_2 physisorption, H_2 chemisorption, H_2 temperature programmed reduction (H_2 TPR) and CO_2 temperature programmed desorption (CO_2 TPD) measurements. The samples are prepared for physisorption measurements by degassing at 1.33 mbar and up to 200 °C. The ad- and desorption isotherms are taken using a liquid nitrogen bath at relative pressures from 0.01 up to 0.99. The specific surface areas of the samples are calculated using the Brunauer–Emmett–Teller (BET) method. For the H_2 TPR experiments samples are dried under flowing Ar at 120 °C for 30 min, cooled down to 50 °C and then the feed is switched to 10% H_2 in Ar. After the Thermal Conductivity Detector (TCD) baseline signal stabilizes, the temperature is increased to 1000 °C with a heating rate of 10 K min^{-1}. The H_2 chemisorption experiments are conducted with the volumetric method. Circa 100 mg of each sample are reduced with H_2 at 200 °C for 4 h and degassed at 300 °C for 6 h. The H_2 adsorption isotherm is recorded at 50 °C. After degassing for 1 h a repeat measurement is taken. The H_2 chemisorption isotherms are used to calculate the active metal surface area using the Langmuir model. The dispersion of active metal D_{Ru} on the catalyst is estimated by multiplying the H_2 uptake of the catalyst Q_{H2} with the molar mass of Ru M_{Ru} *via* eqn (1).

$$D_{Ru} = Q_{H_2} \cdot M_{Ru} \quad (1)$$

The CO_2 TPD experiments are conducted by *in situ* drying of circa 100 mg of sample at 105 °C for 10 minutes under flowing Ar. Then the sample is reduced by 10% H_2 in Ar at 200 °C for 4 h. After reduction, the sample is cooled down to 50 °C and flushed with Ar until a stable TCD baseline signal is achieved. The gas flow is then switched to CO_2 (4.5 purity, MTI Industriegase AG) and the sample is saturated with CO_2 for 20 minutes. Afterwards the feed is switched to He (5.0 purity, MTI Industriegase AG) to remove physisorbed CO_2. After a stable TCD baseline signal is achieved, the temperature is increased by 10 K min^{-1} up to 500 °C, where it is held for 5 min.

Powder X-ray diffraction (PXRD) patterns of the fresh supports and finished catalysts are performed on a X'Pert MDP Pro (PANanalytical) using CuKα radiation between 5° and 80° 2θ. X-ray photoelectron spectroscopy (XPS) spectra of the as made catalysts are recorded on a PHI 5800 (Physical Electronics). Transmission electron microscopy (TEM) images of the finished catalysts are taken using a JEOL 1400 microscope.

2.2 Reaction experiments

All reaction experiments were conducted in a 1/4 inch steel tube with a concentric 1/16 inch inner steel tube to place a K-type thermocouple in the center of the packed catalyst bed. The catalyst bed is fixed with quartz wool and 400 mg of 0.5–0.75 mm silica beads before and after the bed. Previous experiments have shown no detectable blind activity of the setup. H_2 (5.0 purity, MTI Industriegase AG) and CO_2 (4.5 purity, MTI Industriegase AG) are dosed by mass flow controllers (Bronkhorst) at a total flow rate of 50 mL_{STP} min^{-1}. A detailed flowsheet of the setup can be found in the ESI.† 100 mg of catalyst are diluted with 300 mg SiC in the size fraction 150–212 μm and filled into the reactor. The catalyst is reduced *in situ* under flowing H_2 at ambient pressure and 473 K for 8 h.

To gain insights into the (de-)activation behavior of the catalyst, reference conditions are set before and after a parameter variation. Every set of parameters is held for 8 h to ensure enough data points and stable behavior. The temperatures and partial pressures of the individual operating points are shown in Table 1. The reaction program follows seamless after reduction (A) by the first reference condition (B) of 200 °C, 5 barg and

Table 1 Overview of tested process conditions for the screening experiments

	A	B	C	D	E	F	G	H	I	J	K
T/°C	200	200	160	180	200	220	200	200	200	200	200
p_{CO_2}/barg	0	1.25	1.25	1.25	1.25	1.25	1.25	3.125	6.25	2.083	3.125
P/barg	0	5	5	5	5	5	5	12.5	12.5	12.5	12.5

a H_2/CO_2 ratio of 3. For the temperature variation (C–F) the reaction temperature is set to 150 °C and in subsequent 20 K steps increased to 220 °C. After the first variation the process conditions are set to the same values as for "B", now denoted as "G" in order to evaluate deactivation. The next reference point (H) differs from "G" by a higher pressure of 12.5 barg, at which the H_2/CO_2 ratio is varied between 1 and 5 in the following two operating points (I–J). Lastly the same conditions as in "H" are set in "K" again to check for deactivation.

The analysis of the dry product gas is conducted *via* an online gas chromatograph (GC) equipped with a TCD and a flame ionization detector (FID). One sample is taken roughly every 17.5 min and the evaluation of the results is done by taking the mean of the last three samples of the respective operating point. The GC is calibrated to calculate the percentage of C_1–C_6 alkanes. The corresponding unsaturated hydrocarbons can be detected, but are not calibrated.

The conversion of CO_2, X_{CO_2} is calculated from the inlet molar flow rate of CO_2, $\dot{n}_{CO_2,in}$ and outlet molar flow rate, $\dot{n}_{CO_2,out}$ by assuming differential conditions (eqn (2)). With this assumption the conversion is only dependent on the set inlet molar fraction of CO_2, $x_{CO_2,in}$, the outlet molar fractions measured by the FID, x_i and the known carbon number of the corresponding hydrocarbons $n_{i,C}$.

$$X_{CO_2} = \frac{\dot{n}_{CO_2,in} - \dot{n}_{CO_2,out}}{\dot{n}_{CO_2,in}} \approx \frac{\sum_{i=1}^{6} x_i \cdot n_{i,C}}{x_{CO_2,in}} \quad (2)$$

The CO_2 consumption rate r_{CO_2} is calculated normalized to the used catalyst mass m_{cat} according to eqn (3).

$$r_{CO_2} = \frac{\dot{n}_{CO_2,in} \cdot X_{CO_2}}{m_{cat}} \quad (3)$$

The selectivities towards methane and CO are calculated from the GC data by eqn (4).

$$S_i = \frac{x_i}{\sum_{j=1}^{6} x_j \cdot n_{j,C}} \quad (4)$$

As no other products are detected, the selectivity to higher hydrocarbons is calculated according to eqn (5). The index C_{2+} denotes the lumped paraffins and olefins in the carbon number range 2–6.

$$S_{C_{2+}} = 1 - (S_{CH_4} + S_{CO}) \quad (5)$$

Hydrocarbons higher than hexane are not detected.

With the height of the catalyst bed, h_{cat}, the inner diameter of the reactor tube, D_i and the outer diameter of the thermocouple tube, D_e, the bulk density of the catalysts is calculated *via* eqn (6).

$$\rho_b = \frac{\pi}{4}\left(D_i^2 - D_e^2\right) h_{cat} \quad (6)$$

With the bulk density the consumption rate of CO_2 is related to the volume of the catalyst bed by eqn (7).

$$r_{CO_2,V} = r_{CO_2} \cdot \rho_b \quad (7)$$

Due to the low conversion associated with the assumption of differential conditions, the carbon balance is implicitly assumed as closed.

2.3 Kinetic experiments

To gain insight into the reaction network, the results from the reaction experiments are used to design an experiment to determine apparent reaction orders of CO_2 and H_2, as well as the apparent activation energy of the reaction. The three most promising candidates are chosen for this kinetic study. 80 mg of catalyst are used and the total volumetric flow of gas is set to 100 mL_{STP} min^{-1}. The H_2 and CO_2 flow rates are varied with Argon (5.0 purity, MTI Industriegase AG) as balance. The pressure is set to 5 barg. The kinetic test program is shown in Table 2. First the flow rates are set to 50/10/40 mL_{STP} min^{-1} $H_2/CO_2/Ar$ and the temperature is varied from 150 to 190 °C in 20 K steps to determine the activation energy. The first temperature is held for 8 h to ensure stable operation; the other two temperatures are held 4 h. Afterwards the reactant inlet flow composition is varied at 190 °C with 2 h of reaction time as the optimum

Table 2 Overview of tested process conditions for the kinetic experiments, at 5 barg. Flow rates in mL_{STP} min^{-1}

	A	T-variation			p_i-variation							
T/°C	200	150	170	190	190	190	190	190	190	190	190	190
H_2/CO_2	50/0	50/10	50/10	50/10	45/10	45/15	50/15	60/10	60/15	60/20	50/20	45/20
Duration/h	8	8	4	4	2	2	2	2	2	2	2	2

between stable operation and deactivation of the catalyst. For every operating point the last sample from the GC is chosen for evaluation. Measured reaction rates are evaluated by assuming that the power law expression in eqn (8) sufficiently describes the reaction rate r with the partial pressures of CO_2, p_{CO_2} and H_2, p_{H_2} as well as the respective reaction orders, n_{CO_2} and n_{H_2}.

$$r = k \cdot {p_{H_2}}^{n_{H_2}} \cdot {p_{CO_2}}^{n_{CO_2}} \quad (8)$$

The values for the reaction orders and the kinetic constant, k are estimated by fitting the experimentally obtained reaction rates and known partial pressures to eqn (9). With the measured temperatures of the catalyst bed and the determined rate constants, the apparent activation energy is estimated based on the linearized Arrhenius equation, while the Arrhenius plot is established, as well. The turn over frequency (TOF) is calculated by eqn (9) using the H_2 sorption capacity, Q_{H_2} and the mass fraction of Ru, ω_{Ru} to estimate the number of active sites on the catalyst.

$$\mathrm{TOF} = \frac{r_{CO_2} \cdot \omega_{Ru}}{Q_{H_2}} \quad (9)$$

3 Results and discussion

3.1 Catalyst characterization

The physisorption measurements were conducted on the pure supports and on the final catalyst and both measured BET surface areas are compared with the manufacturer specifications in Table 3. The results show that the pure supports are within the manufacturer specifications, with the exception of the activated carbon, and the BET surface area of the catalyst is only slightly below that of the pure support. This shows that the pore structure remains intact after the synthesis procedure and that accessibility of the active material is provided.

Results of H_2 TPR experiments for all catalyst and supports are shown in Fig. 1 for the relevant temperature range. The Ru/C and Ru/CeO_2 catalysts exhibit a much larger TCD-signal than the other samples and are therefore scaled down by a factor of 2 and 3, respectively. Ru/C measurements show a constant and steady increase in H_2 consumption, possibly indicating hydrogenation of the carbon support, making a stable operation of this catalyst in reaction experiments unlikely. Ru/CeO_2 shows two pronounced peaks between 101–119 °C and 141–163 °C indicating the reduction of two different Ru species. All other catalysts show H_2 consumption over a broader range of temperatures, indicating no separation between strongly- and weakly interacting Ruthenium. The silica-supported catalyst shows little H_2 consumption which may indicate strong interaction between the silica and the ruthenium resulting in little reduction at the used temperature or a loss of active material throughout the synthesis procedure. All other catalysts are reducible below 200 °C, which is why this temperature is chosen as the reduction temperature for the chemisorption and reaction experiments. Metallic surface areas and H_2 uptake measured by H_2-chemisorption, as well as estimated dispersions provided in Table 4 show a higher Ru surface area on reducible metal oxides, indicating a better stabilization of the Ru precursor or the metal throughout the synthesis and pretreatment. The silica-supported catalyst shows an especially small metallic surface area again indicating a insufficient stabilization of the active material. By comparing the BET surface area and the Ru surface area and dispersion, it becomes clear that a higher surface area of the support does not automatically result in a higher active surface area and better dispersion.

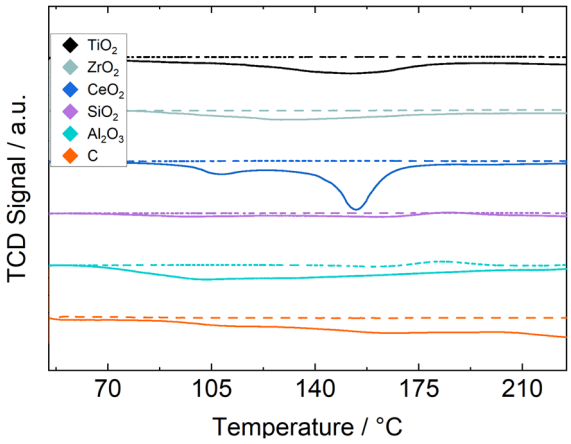

Fig. 1 TCD-signal during H_2 TPR measurements, for pure support (dashed lines) and Ru/support (solid lines).

The CO_2-TPD results for both the catalysts and fresh supports are shown in Fig. 2 to distinguish between desorption peaks from the support and changes due to the supported Ru. Oxygen vacancies on the support enhance the adsorption of CO_2 (ref. 15 and 16) and therefore the addition of Ru might increase the number of adsorption sites on the support due to H_2 spillover. In general the difference between the two signals is not

Table 3 Specific surface areas of the support materials as specified by the manufacturers and determined from our N_2 physisorption measurements evaluated with the BET-method

Material	Specification/$m^2\ g^{-1}$	Pure support/$m^2\ g^{-1}$	Ru/support/$m^2\ g^{-1}$
TiO_2	35–65	55.3 ± 0.3	46.3 ± 0.2
ZrO_2	25–35	32.7 ± 0.1	22.3 ± 0.4
CeO_2	38–42	39.4 ± 0.3	35.9 ± 0.2
SiO_2	350–410	346.7 ± 3.7	232.3 ± 2.0
Al_2O_3	110–150	122.0 ± 0.7	98.7 ± 1.1
C	1100	890.9 ± 28.5	808.1 ± 24.7

Table 4 Active surface areas and H_2 uptake determined from H_2 chemisorption experiments

Catalyst	Metal surface area/$m^2\ g_{cat}^{-1}$	H_2 uptake/μmol g^{-1}	Dispersion/%
Ru/TiO_2	0.96	7.51	7.59
Ru/ZrO_2	5.82	72.6	73.4
Ru/CeO_2	6.57	80.4	81.2
Ru/Al_2O_3	0.24	4.70	4.75
Ru/SiO_2	0.04	0.63	0.64
Ru/C	0.59	4.43	4.47

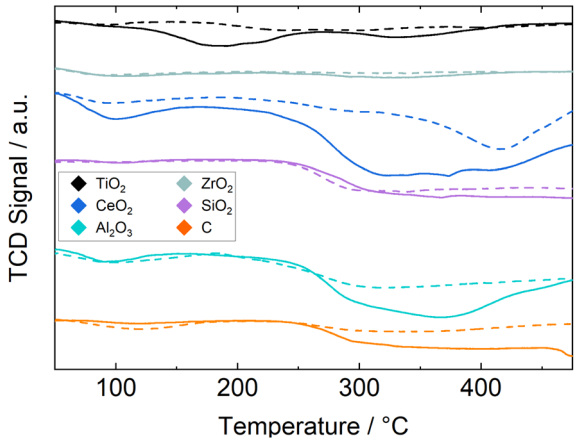

Fig. 2 TCD-signal during CO_2-TPD experiments, for pure support (dashed lines) and Ru/support (solid lines).

large, as the Ru loading is low. Especially for the Ru/ZrO_2 catalyst the two lines barely deviate, indicating either very little adsorption of CO_2 on both support and active material or a strong bonding of CO_2 to ZrO_2 and little bonding to the supported Ru. The only noticeable deviation is detected between 270 and 380 °C. The deviation between the signals is similarly small for the Ru/SiO_2 catalyst with a step change for both catalyst and support at 260 °C. This indicates a large adsorption capacity for CO_2 on SiO_2 and little to no influence from the supported Ru. A similar step-change at 260 °C is seen for the Ru/C catalyst, but not the pure C support, this means that a significant amount of CO_2 adsorbs due to the Ru. The Ru/Al_2O_3 catalyst shows a broad but more defined peak from 250 to 480 °C with a smaller peak at 100–160 °C. The Ru/TiO_2 catalyst shows two distinct peaks at 100–250 °C and 300–390 °C with the former being larger, which is contrary to the other catalysts. The Ru/CeO_2 catalyst shows a large deviation from the signal of the support with two noticeable peaks, the smaller between 80–170 °C and the larger being a step change starting from 260 °C. Here the CeO_2 support also shows a noticeable peak from 350 to 470 °C indicating that much of the large CO_2 capacity is due to the support and the addition of Ru results in more partial reduction of the CeO_2 and thus an increase in CO_2 accepting sites. The two defined H_2 consumption peaks in Fig. 1 support the reduction of more than one surface species and therefore significant reduction of the support as well.

The XPS results (Table 5) are used to analyze the surface composition of the catalysts. The results for the C percentage is unreliable, as the sample holder is a carbon pad and it is shown only for the sake of completion. The XPS results confirm the support as the main component of the catalysts with the respective metal and oxygen exhibiting the largest percentage. The oxygen/metal ratio indicates oxygen excess with respect to the expectations from stoichiometry, which may be explained by the presence of H_2O. The low fraction of Cl for most catalysts shows the efficacy of the ammonia washing, while the low percentage of N shows that NH_3 can subsequently be almost completely removed easily. The comparatively large Cl percentage on Ru/CeO_2 might cause the poisoning of active sites and thus a decrease in activity. The measurements show a low fraction of Ru on the Ru/SiO_2 catalyst, which indicates either a loss of active material, or a significant influence of other effects like wettability or capillary forces, which might lead to migration of Ru to the bulk of the support particles. This would cause Ru being outside of the surface sensitive XPS technique. The Ru amount on Ru/C is much higher than expected, which shows an uneven distribution of Ru on the Ru/C catalyst. Both observations may explain the low dispersion despite the large BET surface area for both the Ru/SiO_2 and Ru/C catalyst.

3.2 Variation of process parameters

The consumption rates of all synthesized catalysts under the process conditions described in Table 1 are shown in Fig. 3. Ru/

Table 5 Surface compositions of all catalysts in atom%. Summarized impurities are: F, Mg, Ca, Fe and P

Material	C	O	Al	Si	Ti	Zr	Ce	N	Cl	Other impurities	Ru
Ru/TiO_2	34.4	46.5	0	0	17.9	0	0	0.57	0.15	0	0.57
Ru/ZrO_2	22.1	53.8	0	0	0	20.4	0	1.09	0.27	0.74	1.55
Ru/CeO_2	14.0	54.3	0	0	0	0	25.0	0.63	2.37	2.21	1.55
Ru/SiO_2	1.38	72.0	0.25	26.2	0	0	0	0	0	0	0.11
Ru/Al_2O_3	17.7	57.5	23.3	0	0	0	0	0.28	0.27	0.67	0.34
Ru/C	61.3	25.9	0	0.94	0	0.31	0	2.74	0.31	1.2	7.26

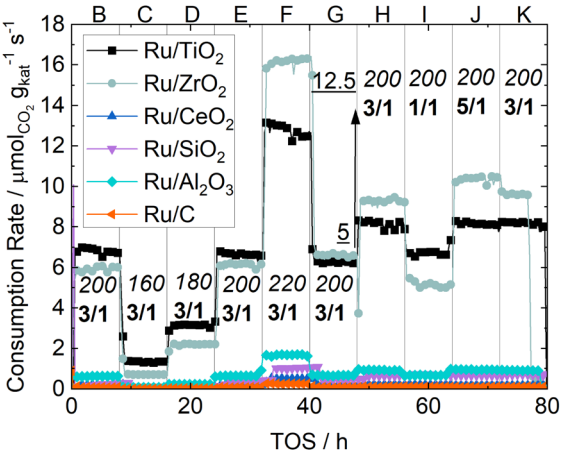

Fig. 3 CO_2 consumption rates of all catalysts under various process conditions as function of TOS. Reduction phase (A) not shown. Points C–F indicate different temperature at 5 barg and H_2/CO_2 ratio of 3 with B and G as reference measurements for deactivation due to temperature variation. Points H–J indicate the variation of the H_2/CO_2 ratio at 12.5 barg and 200 °C with H and K as reference measurements for deactivation due to composition variation. Italic numbers indicate the temperature in degree Celsius, bold numbers the H_2/CO_2 ratio and underlined numbers the switch from 5 barg to 12.5 barg.

TiO_2 and Ru/ZrO_2 are by an order of magnitude the most active catalysts, followed by Ru/Al_2O_3. Among the other catalysts Ru/C is the least active catalyst with activity circa two orders of magnitude lower than the Ru/ZrO_2 catalyst. Generally, the activity of the synthesized catalysts is in the order of $Ru/TiO_2 \approx Ru/ZrO_2 \gg Ru/Al_2O_3 > Ru/SiO_2 > Ru/CeO_2 > Ru/C$. The calculated CO_2 conversion of all catalysts at all operating points is shown in the ESI.† Vannice *et al.*[17] investigated the influence of the support on the CO hydrogenation. In their experiments only Ru/TiO_2 and Ru/Al_2O_3 showed enough activity to produce measurable quantities of methane, which is in line with our results. However, they did not test Ru/ZrO_2 or Ru/CeO_2 catalysts. While the high activity of Ru/TiO_2 has been extensively studied and accredited to a range of metal-support-interaction mechanisms like lattice-matching[18] or the formation of encapsulating overlayers,[19] investigations into Ru/ZrO_2 are scarce. One such study done by Alves *et al.*[20] investigated various ZrO_2 supports and found a high activity, but they did not compare their results with Ru/TiO_2 catalysts. Our results thus show that Ru/ZrO_2 is indeed of comparable or even higher activity than Ru/TiO_2, especially at temperatures above 200 °C. Ru/CeO_2, another reducible metal oxide, displays much lower activity, which is more comparable to Ru supported on the irreducible metal oxides SiO_2 and Al_2O_3. This may be due to the availability of partially reduced sites, which is beneficial to facilitate the adsorption and bond-cleavage of carbon oxides. This bond-cleavage has been proposed before by works like that of Xu *et al.*[19] The low activity of Ru/CeO_2 indicates that the reduction of Ru/CeO_2 catalysts requires careful tuning as noted by Dreyer *et al.*[6] with their experiments using Ru/CeO_2. The low activity here is therefore ascribed to the CeO_2 not being reduced to a sufficient degree under the chosen conditions.

The comparison of the reference points B and G shows that in B Ru/TiO_2 is the most active catalyst and in point G Ru/ZrO_2 is more active than Ru/TiO_2. This steady deactivation of Ru/TiO_2 and a steady activation of Ru/ZrO_2 is most notable at 220 °C, where the consumption rate of the Ru/TiO_2 catalyst noticeable decreases and stays below that of the Ru/ZrO_2 catalyst upon returning to 200 °C. It is also worth noting that for both these catalysts the consumption rate decreases noticeably when the syngas ratio is switched from 3 : 1 to 1 : 1. No effect on conversion is visible for Ru/TiO_2 between H_2/CO_2 ratios of 3 and 5. The influence of the gas composition is much larger for Ru/ZrO_2 when switching to the lowest ratio, while there is a noticeable difference between H_2/CO_2-ratios of 5 and 3. Since the active material is identical, this shows that the support material may change the reaction mechanism through hetero-contacts between the support and active metal in addition to the already studied oxygen-vacancies, which merely accelerate the rate-limiting C–O-bond cleavage.

CO formation is only detected for Ru/CeO_2 and Ru/C. While the general activity of Ru/CeO_2 is low, the selectivity to CO is reliably detected to be around 50% under all process conditions. The activity of Ru/C is so low that the detected amounts of CO are close to the detection limit and the resulting error in selectivity is too large to provide a reliable number. The methane selectivities of all catalyst at the reference points are shown in Table 6. A complete list of selectivities can be found in the ESI.† The catalysts with higher activity show a high selectivity towards methane under all process conditions, while the least active catalyst, Ru/CeO_2 and Ru/C, show a much lower selectivity.

As expected the relationship between temperature and selectivity to methane correlates. Increasing the pressure from reference G to reference H does not influence selectivity towards higher hydrocarbons for the Ru/TiO_2, Ru/ZrO_2 and Ru/CeO_2 catalysts. Temperature measurements show no hot-spot formation which could explain this behavior by thermocatalytic effects. A comparison of the references H and K shows an increase in selectivity towards methane over time for most catalysts, while the activity remains basically the same, even after exposure to a feed composition of H_2/CO_2 of 1. This shows that carbon-rich synthesis gas does not lead to deactivation of any of the catalysts. These results prove that the Ru catalysts used in this study are robust under a broad range of temperatures and CO_2/H_2 ratios.

The small difference in both activity and selectivity when varying the H_2/CO_2 ratio and the moderate influence of increased pressure, shows that an elevated hydrogen partial

Table 6 Methane selectivity in percent of all catalysts at reference operating points during screening experiments

	Ru/TiO_2	Ru/ZrO_2	Ru/CeO_2	Ru/SiO_2	Ru/Al_2O_3	Ru/C
B	96.8	96.4	44.1	98.9	97.4	83.4
G	97.1	96.6	41.9	99.3	97.7	62.4
H	97.3	96.7	50.8	99.0	96.0	77.3
K	97.8	96.8	52.7	99.1	97.4	74.3

pressures is not necessary for low-temperature CO_2 methanation when using ruthenium-based catalysts. This may significantly reduce operating cost as hydrogen and its compression are expected to be at 2 € per kg (ref. 21) and CO_2 at 50 € per tonne in 2040.[22] The significant consumption rates at low temperatures may also allow the use of much more cost-effective and safe heat-management like medium-pressure steam, possibly allowing efficient process-windows inaccessible to other catalysts due to low activity or rapid deactivation. Longer studies and even lower syngas-ratios are necessary to rule out carbon-deposition as a significant deactivation mechanism over extended periods of time.

The consumption rates related to the catalyst bed volume are calculated for the first reference point B *via* the eqn (6) and (7) and shown in Table 7. Due to its higher bulk density, Ru/ZrO_2 has a higher volumetric consumption rate than Ru/TiO_2. This is an important consideration for reactors, where the heat generated per volume is a crucial parameter for design of the thermal management.

3.3 Reaction kinetics

The CO_2 conversion is below 5% for all operating points, which ensures differential conditions. The apparent reaction orders with respect to CO_2, shown in Fig. 4, are practically zero for the Ru/ZrO_2 and Ru/Al_2O_3 catalysts, which is in line with the results from Mansour and Iglesia, who found that the reaction of surface CO is rate-limiting and therefore the reaction rate to be independent of CO_2 pressure.[23] The reaction order for the Ru/TiO_2 catalyst is non-zero, which indicates a different reaction mechanism compared to the other two catalysts, even though the difference is small. The apparent reaction orders with respect to H_2, shown in Fig. 5, are close to 0.5 for the Ru/TiO_2 and Ru/ZrO_2 catalyst, which is in line with those determined by Wang *et al.*[24] in a much more in-depth analysis of the kinetics of a Ru/Al_2O_3 catalyst. Their results found a reaction order of 0.3–0.5 for H_2. The reaction order of H_2 for the Ru/Al_2O_3 catalyst in this study is 0.25 and therefore below that expected from literature. The different H_2 reaction order of the Ru/Al_2O_3 catalyst compared to the other catalysts may indicate a different reaction mechanism when comparing Ru/Al_2O_3 to Ru/TiO_2 and Ru/ZrO_2.

The Arrhenius-plot for the investigated catalysts is shown in Fig. 6. The experiments of Wang *et al.*[24] found activation energies between 57 and 80 kJ mol^{-1} depending on the H_2/CO_2 ratio. At a ratio of 5, as was used here, the resulting activation energy

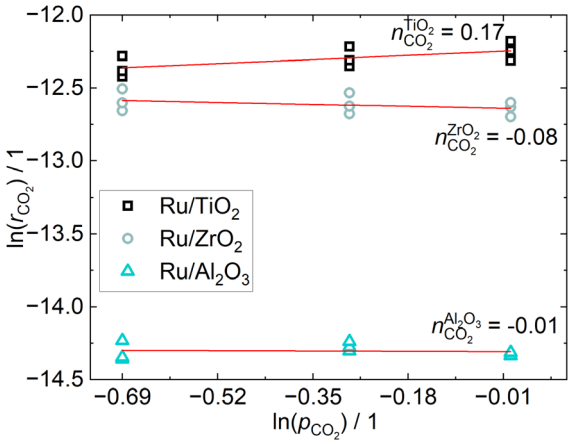

Fig. 4 Reaction orders of CO_2 obtained from a linear fit of the consumption rates calculated according to 9 at three different constant H_2 pressures.

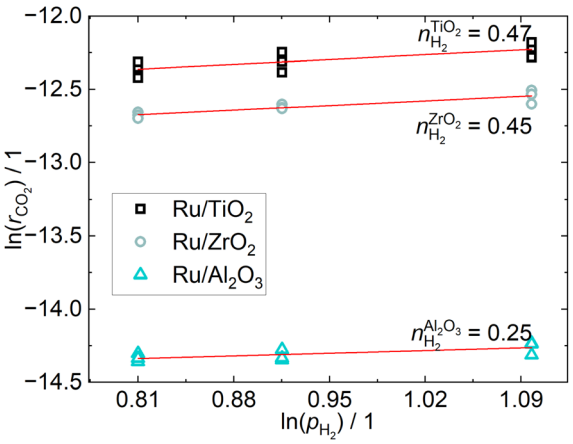

Fig. 5 Reaction orders of H_2 resulting from a linear fit through the consumption rates calculated from varying the H_2-partial pressure at three different constant CO_2 pressures.

was 78 kJ mol^{-1} for their 5% Ru/Al_2O_3 catalyst, while it is 58 kJ mol^{-1} for 0.5% Ru/Al_2O_3, which is well in line with the Ru/TiO_2 and Ru/Al_2O_3 catalysts in this study. The activation energy for our Ru/ZrO_2 catalyst is much higher than the TiO_2 and Al_2O_3 supported Ru in this study, indicating a different reaction mechanism on Ru/ZrO_2 compared to the other two catalysts. This solidifies the indication of different reaction mechanisms depending on the chosen support.

Table 7 Bulk density, consumption rates and volumetric consumption rates at the first reference point for all catalysts

Catalyst	Bulk density/g cm^{-3}	Consumption rate/μmol g_{cat}^{-1} s^{-1}	Volumetric consumption rate/μmol cm^{-3} s^{-1}
Ru/TiO_2	0.34	6.75	2.28
Ru/ZrO_2	0.44	6.07	2.70
Ru/CeO_2	0.34	0.20	0.07
Ru/Al_2O_3	0.30	0.63	0.19
Ru/SiO_2	0.23	0.31	0.07
Ru/C	0.35	0.09	0.03

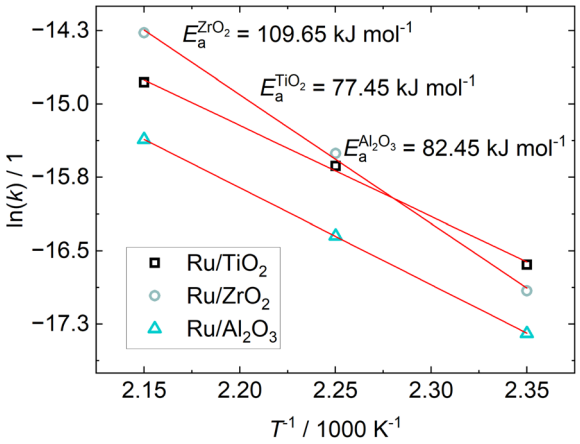

Fig. 6 Arrhenius-plot from the kinetic constant obtained from parameter fitting *via* eqn (8) and the resulting apparent activation energy for different catalysts.

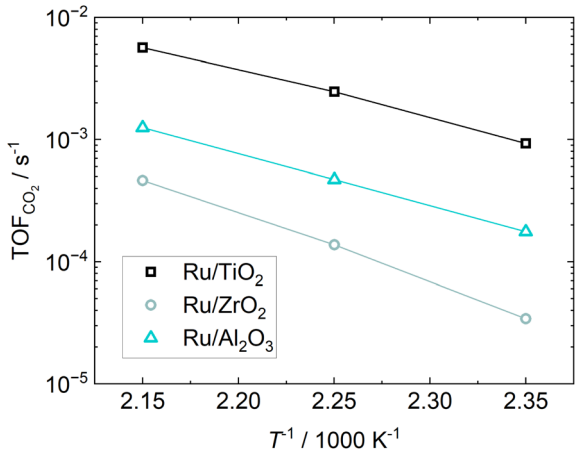

Fig. 7 Arrhenius-plot based on the TOF from CO_2 consumption rate.

The TOF during temperature variation calculated *via* eqn (9), shown in Fig. 7, highlights Ru/TiO_2 as the most active catalyst.

The TOF of 5.7×10^{-3} s^{-1} for the Ru/TiO_2 catalyst at 190 °C is well in line with our previous results[13] and slightly below the value of 5 to 10×10^{-3} s^{-1} measured by Abdel-Mageed *et al.*[10] Chen *et al.*[25] investigated a 2.3 wt% Ru/Al_2O_3 catalyst and at 190 °C found TOFs of 4×10^{-4} s^{-1} and 6.8×10^{-3} s^{-1}, depending on the pretreatment of the catalyst. The TOF of 1.3×10^{-3} s^{-1} at 190 °C of the Ru/Al_2O_3 catalyst in this study is in good agreement with the TOF achieved by Chen *et al.* The same group also investigated a 2.1 wt% Ru/ZrO_2 catalysts[26] and at 190 °C found a TOF of 3.4×10^{-3} s^{-1}, which is much higher than the 4.6×10^{-4} s^{-1} measured in this study. This may be due to the assumption that H_2 only chemisorbs on Ru. In particular, the spillover of hydrogen atoms onto the support is a known phenomenon,[27] which may lead to H_2 at both the Ru and support surface. This might explain the large measured H_2 capacity of the catalysts using partially reducible metal oxides as supports, which would result in overestimating the active surface area and dispersion and consequently to the underestimation of the TOF. The reported TOFs and literature data are summarized in Table 8.

Table 8 Summary of TOF values from this work and from literature

Catalyst	In this work/10^{-3} s^{-1}	In literature 10^{-3} s^{-1}
Ru/TiO_2	5.7	5 to 10 (ref. 13 and 10)
Ru/ZrO_2	0.5	3.4 (ref. 26)
Ru/Al_2O_3	1.3	0.4 to 6.8 (ref. 25)

4 Conclusions

In this work we tested various Ru-based catalysts using commercial support materials under mild process conditions to find the most promising catalyst and process conditions for a safe and sustainable CH_4 synthesis from CO_2. The results highlight Ru/TiO_2 as the most active catalyst with high activity even at low temperatures. The catalyst remains stable even at elevated CO_2 concentrations with high CH_4 selectivity. The kinetic parameters determined for the Ru/TiO_2, Ru/ZrO_2 and Ru/Al_2O_3 catalysts give an indication that the reaction mechanism for each of these catalysts may differ from the others to a certain extent. Since the main difference between these catalysts is the support material, the significant influence of metal-support interactions in governing the activity of the catalyst is revealed. The activity of the TiO_2, ZrO_2 and Al_2O_3 supported catalysts are not just a morphological effect due to high metal surface areas, but possibly a mechanistic effect originating from the interaction of Ruthenium with the support materials.

The results obtained for the unexplored low temperatures and H_2/CO_2 ratios indicates potentially attractive process windows by reducing the cost of thermal management and H_2 from electrolysis by leveraging sub-stoichiometric H_2/CO_2 ratios. The results of kinetic experiments show that the reaction mechanism must be influenced by the support material, highlighting the need for catalyst specific optimization strategies for metal-support interactions. The low temperatures employed during calcination and reduction of the catalyst show that the higher temperatures often employed for both steps may not be necessary.

The comparative nature of the materials and wide process window tested in this study makes it an ideal basis for future studies of more sophisticated catalyst materials or for CO_2 hydrogenation at mild conditions. Finally, the results also show that the most promising Ru-based catalysts for CO_2 hydrogenation are supported on either ZrO_2 or TiO_2.

Data availability

The data supporting this article have been included as part of the ESI.†

Author contributions

Göran Baade: conceptualization, investigation, methodology, visualization, writing – original draft preparation. Jens Friedland: methodology, writing – reviewing and editing. Koustuv Ray: writing – reviewing and editing. Robert Güttel: conceptualization, funding acquisition, methodology, project administration, resources, supervision, writing – reviewing and editing.

Conflicts of interest

There are no conflicts to declare.

Acknowledgements

The authors would like to thank the Vector Stiftung for funding this project (P2022-0013) and the Deutsche Forschungsgemeinschaft for funding the experimental setup within the Major Research Instrumentation Programme (INST 40/516-1 FUGG) as well as IBU-tec advanced materials AG for providing the ZrO_2 and CeO_2 support, Evonik Industries AG for providing the TiO_2, Al_2O_3 and SiO_2 support and Infiltec GmbH for providing the C support. Additionally we would like to thank Samuel Blessing of the Institute of Inorganic Chemistry II at Ulm University for conducting the PXRD measurements and Konstantin Schüttler of the Institute of Surface Chemistry and Catalysis at Ulm University for conducting the XPS measurements.

Notes and references

1 D. A. Lashof and D. R. Ahuja, *Nature*, 1990, **344**, 529–531.
2 UN-DESA, *The Sustainable Development Goals Report 2023: Special Edition*, 2023, **https://unstats.un.org/sdgs/report/2023/**.
3 L. Jiang, W. Liu, R. Wang, A. Gonzalez-Diaz, M. Rojas-Michaga, S. Michailos, M. Pourkashanian, X. Zhang and C. Font-Palma, *Prog. Energy Combust. Sci.*, 2023, **95**, 101069.
4 S. Rönsch, J. Schneider, S. Matthischke, M. Schlüter, M. Götz, J. Lefebvre, P. Prabhakaran and S. Bajohr, *Fuel*, 2016, **166**, 276–296.
5 J. Ilsemann, M. M. Murshed, T. M. Gesing, J. Kopyscinski and M. Bäumer, *Catal. Sci. Technol.*, 2021, **11**, 4098–4114.
6 J. A. Dreyer, P. Li, L. Zhang, G. K. Beh, R. Zhang, P. H.-L. Sit and W. Y. Teoh, *Appl. Catal., B*, 2017, **219**, 715–726.
7 S. Scirè, C. Crisafulli, R. Maggiore, S. Minicò and S. Galvagno, *Catal. Lett.*, 1998, **51**, 41–45.
8 C. Wang, H. Sun, X. Liu, X. Jin, Y. Feng, H. Shi, D. Wang, Y. Zhang, Y. Wang and Z. Yan, *Fuel*, 2023, **345**, 128238.
9 Z. Zhao, Q. Jiang, Q. Wang, M. Wang, J. Zuo, H. Chen, Q. Kuang and Z. Xie, *ACS Sustain. Chem. Eng.*, 2021, **9**, 14288–14296.
10 A. M. Abdel-Mageed, K. Wiese, M. Parlinska-Wojtan, J. Rabeah, A. Brückner and R. J. Behm, *Appl. Catal., B*, 2020, **270**, 118846.
11 C. Tébar-Soler, V. M. Diaconescu, L. Simonelli, A. Missyul, V. Perez-Dieste, I. Villar-García, D. Gómez, J.-B. Brubach, P. Roy, A. Corma and P. Concepción, *ACS Catal.*, 2024, **14**, 4290–4300.
12 A. Aitbekova, E. D. Goodman, L. Wu, A. Boubnov, A. S. Hoffman, A. Genc, H. Cheng, L. Casalena, S. R. Bare and M. Cargnello, *Angew. Chem., Int. Ed.*, 2019, **58**, 17451–17457.
13 H. Becker, D. Ziegenbalg and R. Güttel, Preprint: Photoassisted amplification of chain-growth in CO_2 hydrogenation: Switching selectivities of heterogeneously catalyzed reactions with light, 2024, **https://www.chemrxiv.org/engage/chemrxiv/article-details/65e822589138d23161c69590**.
14 J. M. Crawford, B. E. Petel, M. J. Rasmussen, T. Ludwig, E. M. Miller, S. Halingstad, S. A. Akhade, S. H. Pang and M. M. Yung, *Appl. Catal., A*, 2023, **663**, 119292.
15 J. Niu, C. Zhang, H. Liu, Y. Jin and R. Zhang, *Front. Energy*, 2023, **17**, 545–554.
16 X. Yan, C. Duan, S. Yu, B. Dai, C. Sun and H. Chu, *J. CO_2 Util.*, 2024, **79**, 102648.
17 M. Vannice, *J. Catal.*, 1982, **74**, 199–202.
18 J. Zhou, Z. Gao, G. Xiang, T. Zhai, Z. Liu, W. Zhao, X. Liang and L. Wang, *Nat. Commun.*, 2022, **13**, 327.
19 J. Xu, X. Su, H. Duan, B. Hou, Q. Lin, X. Liu, X. Pan, G. Pei, H. Geng, Y. Huang and T. Zhang, *J. Catal.*, 2016, **333**, 227–237.
20 L. M. Alves, M. P. Almeida, M. Ayala, C. D. Watson, G. Jacobs, R. C. Rabelo-Neto, F. B. Noronha and L. V. Mattos, *Chem. Eng. Sci.*, 2021, **239**, 116604.
21 T. Terlouw, C. Bauer, R. McKenna and M. Mazzotti, *Energy Environ. Sci.*, 2022, **15**, 3583–3602.
22 M. Fasihi, O. Efimova and C. Breyer, *J. Cleaner Prod.*, 2019, **224**, 957–980.
23 H. Mansour and E. Iglesia, *J. Am. Chem. Soc.*, 2021, **143**, 11582–11594.
24 X. Wang, Y. Hong, H. Shi and J. Szanyi, *J. Catal.*, 2016, **343**, 185–195.
25 S. Chen, A. M. Abdel-Mageed, M. Dyballa, M. Parlinska-Wojtan, J. Bansmann, S. Pollastri, L. Olivi, G. Aquilanti and R. J. Behm, *Angew. Chem., Int. Ed.*, 2020, **59**, 22763–22770.
26 S. Chen, A. M. Abdel-Mageed, M. Li, S. Cisneros, J. Bansmann, J. Rabeah, A. Brückner, A. Groß and R. J. Behm, *J. Catal.*, 2021, **400**, 407–420.
27 R. Prins, *Chem. Rev.*, 2012, **112**, 2714–2738.